Order−Order Phase Transition between Spherical and Cylindrical Microdomain Structures of Block Copolymer. I. Mechanism of the Transition

Kohtaro Kimishima,[†,§] Tadanori Koga,[†,||] and Takeji Hashimoto*[,†,‡]

Hashimoto Polymer Phasing Project, ERATO, Japan Science and Technology Corporation, and Department of Polymer Chemistry, Graduate School of Engineering, Kyoto University, Kyoto 606-8501, Japan

Received August 27, 1999

ABSTRACT: The mechanism of the order−order transition in a block copolymer between spheres in a body-centered cubic lattice (bcc-spheres) and hexagonal cylinders was investigated by means of small-angle X-ray scattering (SAXS). The block copolymer studied is a polystyrene-*block*-polyisoprene diblock copolymer having a molecular weight of 4.40×10^4 and a weight fraction of polystyrene of 0.20. Cylindrical microdomains on a hexagonal lattice were observed up to 114.7 °C and changed to bcc-spheres above 116.7 °C. The OOT transition between the two microdomains reversibly occurred. Moreover, the repetitive OOT process (defined in the text) occurred with conservation of the grain structures and of orientation of the crystallographic axes in the grains. When the SAXS pattern from a single grain was examined, it was found that the cylinders are transformed into a series of spheres with the cylindrical axes corresponding to the [111] direction of the bcc-spheres upon heating and that the spheres along the [111] direction of the bcc lattice are deformed and interconnected to cylinders upon cooling, both without changing the grain structures.

I. Introduction

Themoreversible order−order transition (OOT) between different kinds of the microdomain structures of a block copolymer in a weak segregation limit was predicted by Leibler[1] 2 decades ago, and recently some experimental results on the OOT have been reported. It is no doubt that the block copolymer exhibits OOT. However the detail processes and mechanisms of the transition have not been thoroughly understood. In this series of papers, we focus on the thermoreversible transition between spherical and cylindrical microdomain structures in a polystyrene-*block*-polyisoprene (PS−PI) diblock copolymer melt and try to elucidate the transition mechanism and the dynamic behavior.

It is well-known that a block copolymer consisting of mutually immiscible polymers form microdomain structures such as alternating lamellar, cylindrical, and spherical microdomains. In the strong segregation limit, the morphology basically depends on the volume fraction of one of the constituent block chains[2−4] (f, block composition), and there were many previous works classifying the morphologies in terms of f. On the other hand, according to Leibler's theory, the morphology depends not only on f but also on the quantity χN, where χ and N are Flory's segmental interaction parameter between the constituent polymers in block copolymers and the total degree of polymerization, respectively. The theory predicts the equilibrium morphology changes from lamellae to spheres through cylinders and eventually to a disordered state with decreasing χN, except for the block copolymer having $f = 0.5$. Since χ depends on the temperature, the thermoreversible transition was expected. For a while, this prediction had not been experimentally confirmed. However, recently the OOTs of block copolymer have been successively reported.[5−13]

Sakurai et al. reported the thermoreversible OOT between spheres in a body-centered cubic lattice (bcc-spheres) and hexagonal cylinders for a PS−PI diblock copolymer[5] and its diocthylphthalate (DOP) solutions[6] with varied polymer concentrations based on small-angle X-ray scattering (SAXS) and/or transmission electron microscopy (TEM) studies. At higher temperature they observed the bcc-spheres, while if temperature was lowered hexagonally packed cylindrical microdomains appeared, and this transition was thermally reversible. The transition temperature lowered with decreasing polymer concentrations, indicating the transition point depends on the χN alone for a constant f.

Bates and co-workers first presented the complex phase behavior near the order−disorder transition (ODT) using a series of poly(ethylenepropylene)-*block*-poly(ethylethylene) (PEP−PEE)[7] and PS−PI diblock copolymers.[8,9] They identified new morphology such as a hexagonally perforated layers (HPL) and a bicontinuous cubic phase having an $Ia\bar{3}d$ space group symmetry (gyroid) using various methods; dynamic mechanical measurements, TEM, SAXS, and small-angle neutron scattering (SANS). The gyroid structure was also identified by Hajduk et al.,[10] using SAXS, TEM, and computer simulations. They observed lamellar microdomains in a PS−PI diblock copolymer consisting of 37 wt % PS at 115 °C. After annealing the sample at 150 °C, which was approximately 50 °C below the ODT temperature, they observed that the microdomains were transformed into gyroid structures. The thermoreversibility between lamellar and gyroid structures was also examined. The complete conversion from the gyroid into lamellar microdomains did not occur even after a long-time annealing over 20 h at 100 °C; however, a partial conversion was observed by both TEM and SAXS,

* To whom correspondence should be addressed.
† Japan Science and Technology Corporation.
‡ Kyoto University.
§ Present address: Tonen Chemical Corp., 3-1, Chidori, Kawasaki-ku, Kanagawa 210-0865, Japan.
|| Present address: Department of Chemistry, State University of New York at Stony Brook, Stony Brook, NY 11794-3400.

10.1021/ma991470k CCC: $19.00
Published on Web 01/22/2000

showing the nature of the thermoreversibility between gyroid and lamellar morphologies. The authors also reported the thermoreversible OOT between lamellar and cylindrical microdomains in a polystyrene-*block*-poly(ethene-*co*-butene) diblock copolymer by SAXS and TEM.[11]

These experimental reports on OOT have been stimulated by the theoretical studies on the phase diagram of block copolymer melt. The experimental results, in turn, are expected to promote further the theoretical studies. Leibler's mean-field theory[1] based on the random phase approximation[14] (RPA) is invalid under a strong or an intermediate segregation limit since it assumed weak segregation. Actually the phase boundaries between different mesophases do not agree with the experimental results.[3] The strong segregation theory (SST) developed by Helfand et al.[15] predicts the experimental phase boundaries but does not predict OOT upon changing temperature at a given f. A theory covering for a weak to a strong segregation was proposed by Ohta and Kawasaki[16] based on the generalized Landau−Ginzburg theory and by Whitmore and Vavasour[18] based on self-consist field theory (SCFT). The effects of thermal fluctuations on the phase diagram and the phase transition mechanism were discussed by Fredrickson and Helfand.[17] The recent theoretical reviews are presented by Matsen and Bates[19] and in it they reported the phase diagram using a full SCFT without traditional assumptions. The further accumulations of experimental results on OOT are desired for deeper understanding of the physics underlying OOT.

The study of the microdomain structure under the weak-to-intermediate segregation limit has been remarkably advanced both experimentally and theoretically. However, little has been clarified about the transition process and the dynamics. Understanding the OOT mechanism could provide the way for controlling the orientation of the microdomains. For example, the gyroid structure seems rather difficult to orient due to the connectivity of both phases. If one has a block copolymer showing the OOT between lamellae and gyroid (as already reported[10]) and knows the spatial relation between the two structures before and after the OOT, the problem is reduced to spatially aligning lamellae, which has been already achieved by using shear flow, for example. Also in the practical applications, the dynamics of OOT may become very important to control the morphology during a limited processing time.

In the present paper, we are concerned with the process of thermoreversible OOT between spheres and cylinders as a simple case. Though the OOT itself has already been reported,[5,6,12] the detailed transition process has not yet been elucidated. To investigate the intermediate structure developed during the OOT, TEM observation is powerful as Hadjuk et al. applied it to the OOT between lamellae and cylinders.[11] However this method required freezing the sample during the OOT and did not enable an in situ investigation of the OOT process. For the in situ investigation, the scattering experiment is superior to the TEM experiment. In the conventional scattering experiments, the size of the incident beam on the sample is quite large compared with the size of the grains within which the ordered microdomain structure exists in a coherent orientation. Therefore, the observed scattering pattern is a summation of the scattering from many grains. If the orientation of the grains is perfectly random, the scattering pattern should be circularly symmetric with respect to the incident beam, giving rise to circular diffraction rings. However, if the size of the grain becomes large enough and comparable to the beam size, Bragg's scattering peaks are observed as diffraction spots. By determining the positions of the diffraction spots, one is able to know the orientation of the microdomain structures and corresponding lattice planes in the single grain that one is focusing on. If one can follow time changes in the diffraction spots during the OOT, one can follow the mechanism and process of OOT in the single grain. Though there are many previous works which are concerned with developing of large grains by shear flow,[12,13,20,21] in this work we tried to develop a large grain with a slow cooling of the specimen in order to minimize the external field affecting the transition scheme, if there were such effects.

II. Sample and Experimental Method

The sample used in this study was a PS−PI diblock copolymer prepared by living anionic polymerization with *sec*-butyllithium as an initiator and cyclohexane as a solvent. The number-averaged molecular weight, M_n, determined by GPC (HLC-8020, THOSO, Co. Ltd.) is 4.39×10^4 and the polydispersity index, M_w/M_n, is 1.02 with M_w being the weight-averaged molecular weight. The weight fraction of PS determined by ^{1}H NMR (JMR-400, JEOL, Co. Ltd.) is 0.204 ± 0.005. The diblock copolymer was dissolved into toluene with a small amount of antioxidant (BHT) and cast into film specimens from a 5% polymer solution. The film specimens thus obtained were then dried under vacuum until no further weight loss was observed.

SAXS measurements were conducted with an apparatus consisting of an 18 kW rotating-anode X-ray generator (M18XHF−SRA, MAC Science Co. Ltd.) with a graphite crystal monochromator to obtain the Cu Kα beam with a wavelength of 0.1542 nm, a collimator, a vacuum chamber for the incident-beam path and scattered-beam path, and a detector. The SAXS profiles were measured using a one-dimensional position-sensitive proportional counter (PSPC) with line focus optics and were corrected for the absorption of the sample, background scattering, and thermal diffuse scattering arising from the acoustic phonons. Two-dimensional (2D) SAXS patterns were also measured with a pinhole collimation and a two-dimensional imaging plate[22] (IP)(DIP-220, MAC Science, Co. Ltd.).

The grain structure of the sample was observed by a polarized-light optical microscopy equipped with a cooled CCD (C5985, Hamamatsu Photonics, Co. Ltd.) for a detector. To minimize an overlapping of the optical image along the thickness direction, the thin sample having a thickness of 0.1 mm was used. The thin specimen was placed on a heating stage (THMS-600, LINKAM Scientific, Co. Ltd.) controlled at various temperatures within an accuracy of ±0.1 K. Observation was carried out under nitrogen atmosphere to avoid thermal degradation of the sample.

III. Results

III-1. Phase Behavior and Phase Transition Temperature. In Figure 1 typical SAXS profiles of the block copolymer measured at various temperatures were plotted in double logarithmic scale against the magnitude of the scattering vector, q, defined by $q = (4\pi/\lambda)\sin(\theta/2)$ with λ and θ being the wavelength of the incident X-ray and the scattering angle, respectively. Measurements were carried out in a cooling process from 177.4 °C. Before we measured the SAXS profile at a given temperature, we waited for 40 min after attaining that temperature. Then the intensity distribu-

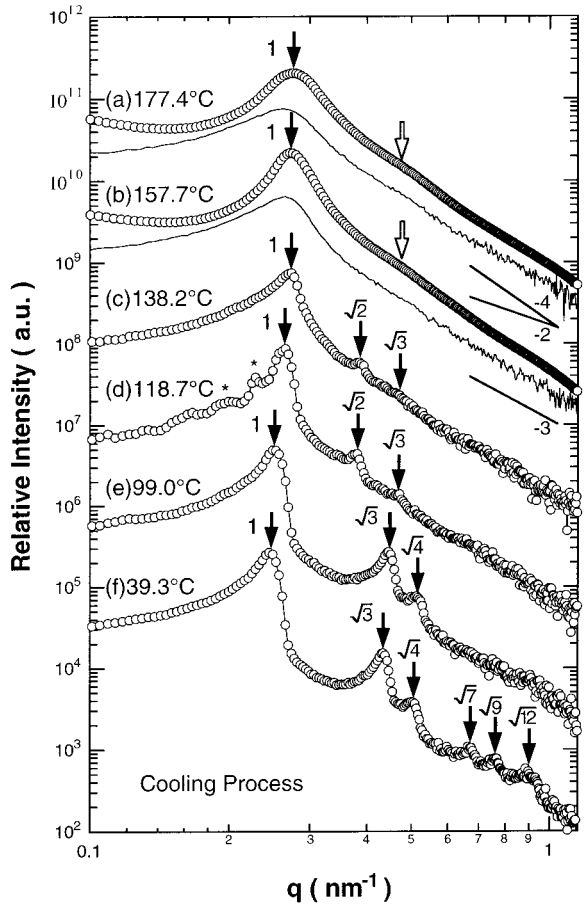

Figure 1. SAXS profiles of the block copolymer taken with PSPC, showing the lattice-disordered spheres (LDS) at (a) 177.4 °C and (b) 157.7 °C (the profiles shown by markers and solid lines are desmeared and smeared profiles, respectively, while other profiles in the figure are smeared profiles), the spheres on a body-centered cubic lattice (bcc-sphere) at (c) 138.2 °C and (d) 118.7 °C, and the cylinders on a hexagonal lattice (hex-cylinder) at (e) 99.0 °C and (f) 39.3 °C. The profiles from parts a to f were obtained in a cooling process. The peaks marked with an asterisk in profile d are the smeared peaks from the large grains as discussed in the text.

tion was accumulated for 30 min, and the sample temperature was lowered stepwise to the next one and kept at that temperature for 40 min before the next SAXS measurement. An average cooling rate corresponding to this cooling scheme was about 15 K/h.

The profiles a and b, plotted by open marker, obtained at 177.4 and 157.7 °C, respectively, are corrected for slit-width and height smearings. They show a broad first-order scattering maximum (marked by a black arrow) and a shoulder at around $q = 0.45$ nm^{-1} (marked by a white arrow). To ensure the shoulder was not an artifact brought by an error in the desmearing correction, the smeared profiles are also presented by solid lines under each desmeared profile. A close examination of the smeared profiles indicates existence of the shoulder. The scattering intensity at high q obey approximately the power law of q^{-4} for the desmeared profiles, indicating a well-defined interface exists between the two microphases (Porod's law[23]). Note that the asymptotic behavior of q^{-4} is observed as q^{-3} in the smeared profiles with a relative long slit.[24] In the disordered state where the block copolymers are mixed on a molecular level, the desmeared scattering intensity decrease with q^{-2} at high q.[1] The results at 177.4 and 157.7 °C do not satisfy this criterion and reveal that the block copolymer at these temperatures forms microdomains with only a short-range order: the microdomains with a well-defined interface exists, though the microdomains are not arranged with a long-range order. This observation is consistent with those reported by Sakamoto et al.[25] This state is different from the disordered state where the PS and PI block chains are mixed on a molecular level and forming the dynamical thermal concentration fluctuations. The domainlike structures which may be generated by the thermal fluctuations in the disordered state are dynamic objects and are expected to have no clear interface.

At temperatures at 138.2 and 118.7 °C (profiles c and d), the higher-order scattering maxima were observed at positions of $\sqrt{2}$ and $\sqrt{3}$ relative to that of the first-order scattering maximum at the scattering vector q_m, indicating formation of spherical microdomains packed in a body-centered cubic lattice (hereafter denoted as bcc-sphere).[26] Leibler's theory predicts that the disordered state is transformed into the bcc-sphere when the value of χ is increased. In this sense, the structures at 157.7 and 177.4 °C (profiles a and b) are expected to exhibit the disordered state since χ between PS and PI, χ_{SI}, decreases with elevating the temperature. However, profiles a and b show existence of the microdomains (possibly spherical microdomains) with a well-defined interface but with no long-range order as mentioned before as a structural entity persisting over the time scale of the SAXS experiments. Thus, we considered the structure is a "lattice-disordered sphere" (LDS), where the bcc lattice was distorted by thermal fluctuations. We note here this type of melting transition between the bcc-sphere and the LDS was also observed by Schwab et al.[27] and Sakamoto et al.[25] in PS−PI diblock copolymer and PS−PI−PS triblock copolymer, respectively, showing the universality of the LDS structure.

The positions of the higher-order scattering maxima with respect to q_m changed to $\sqrt{3}$, $\sqrt{4}$ below 99.0 °C (profiles e and f). With decreasing temperature the, higher-order scattering maxima became more pronounced, which is due to the fact that χ_{SI} gets larger. At 39.3 °C the higher-order peaks at least up to $\sqrt{12}q_m$ appeared. Their relative positions of $\sqrt{3}$, $\sqrt{4}$, $\sqrt{7}$, $\sqrt{9}$, and $\sqrt{12}$ indicates the microdomain structure changed to cylindrical microdomains on a hexagonal lattice (hereafter denoted as hex-cylinder). Since the measurement was carried out in the cooling process from a high temperature, this morphological transition was not considered to be a nonequilibrium effect encountered by solution casting. Any nonequilibrium effects on the morphology in the as-cast film should be relaxed by annealing the film at the high temperatures covered in this experiment.

To confirm the thermoreversibility between the bcc-sphere and the hex-cylinder and determine the accurate transition temperature, a SAXS experiment with a small temperature increment or decrement was carried out in both heating and cooling processes. Parts a and b of Figure 2 show the SAXS profiles taken with PSPC in a heating process and a cooling process, respectively. Here we deliberately show only the smeared profiles in order to avoid any artifacts that might be brought by the desmearing process. First in the heating process (left side of the figure) the measurement was started from 99.0 °C where the hex-cylinder was observed. Upon increasing temperature with about a 2 K increment, the SAXS profiles at each temperature were measured for

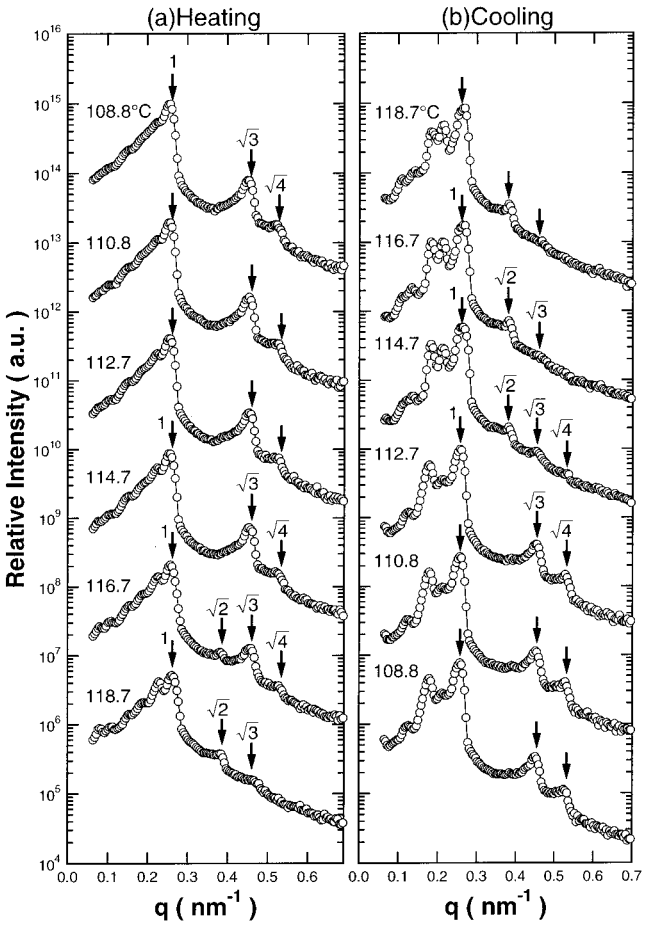

Figure 2. Smeared SAXS profiles taken with PSPC measured in (a) a heating process and (b) a cooling process, respectively. We found that the thermoreversible transition between the bcc-sphere and the hex-cylinder started to occur between 114.7 and 116.7 °C in both processes.

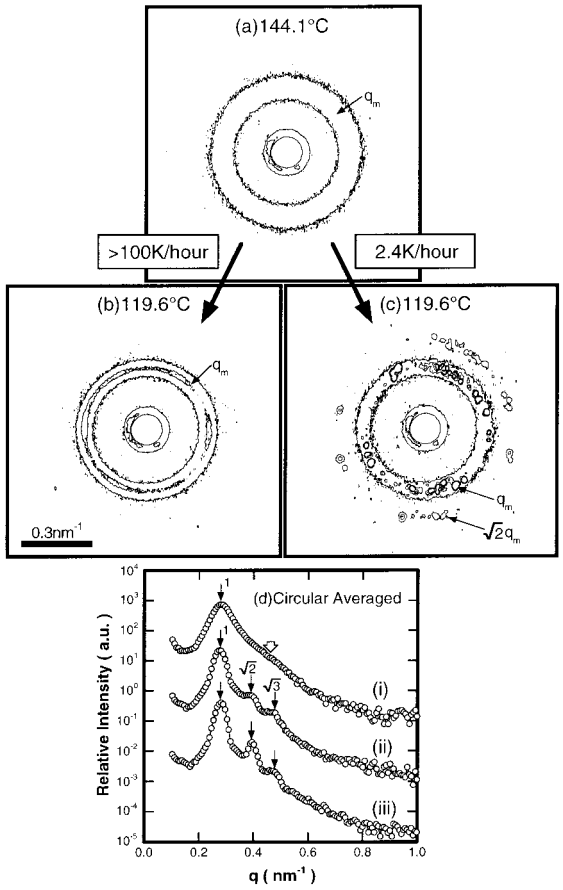

Figure 3. SAXS patterns taken with IP at (a) 144.1 °C for the LDS structure and at (b and c) 119.6 °C for the bcc-sphere. The patterns a−c show contour patterns (isointensity lines). Cooling the sample with a slow rate from the LDS to the bcc-sphere developed the relatively large grains in the sample, which is identified by the observation of the spotlike diffraction peaks (pattern c), while the scattering from the sample with a rapid cooling shows an almost isotropic pattern (pattern b). Profiles i, ii, and iii in part d are the circularly averaged profiles of patterns a, b, and c, respectively.

30 min after waiting for 40 min since the preset temperature had been attained. Then the temperature was increased to the next one and the measurement was started according to the same scheme as described above. An average heating rate corresponding to this process was 0.8 K/h. Only few profiles around the OOT were presented in the figure. Up to 114.7 °C, the higher order scattering maxima of $\sqrt{3}q_m$ and $\sqrt{4}\ q_m$ were observed, indicating existence of the hex-cylinder.[26] At 116.7 °C the second-order scattering maximum appeared at $\sqrt{2}q_m$ and the further higher-order scattering maxima appeared at $\sqrt{3}q_m$ and $\sqrt{4}q_m$. The scattering maxima appeared only at $\sqrt{2}q_m$ and $\sqrt{3}q_m$ at 118.7 °C, indicating that the morphological transition from the hex-cylinder to the bcc-sphere started to occur between 114.7 and 116.7 °C.

After the measurement was continued up to 150 °C, the cooling measurement was carried out with a 2 K decrement (Figure 2b). Down to 116.7 °C the profiles indicated the bcc-sphere, and the change in the relative positions of the higher-order scattering peaks started at 114.7 °C and were completed at 112.7 °C, below which the profiles show the hex-cylinder. Thus, the morphological transition between the bcc-sphere and the hex-cylinder started to occur between 114.7 and 116.7 °C in both the heating and cooling processes. Thus, the order−order transition temperature, T_{OOT}, starts at about 115.7 °C and occurs over a temperature width of 2 K.

We note here the glass transition temperature of PS microdomains of the block copolymer was determined to be 65 °C by differential scanning calorimeter (DSC) which is 50 °C below T_{OOT}, confirming that the transition occurs in molten state.

III-2. Development of the Relatively Large Grains. In some profiles shown in Figure 1 and Figure 2, unusual scattering peaks at $q < q_m$ were observed (for example, see the peaks marked by an asterisk in profile d of Figure 1), which appeared as a consequence of the smearing effect (smeared peaks). If the scattering is circularly symmetric with respect to the incident beam, the scattering peaks are smoothly smeared. However, when the spotlike scattering patterns from relatively large grains are detected with a line focused beam, a smeared peak or peaks appeared at $q < q_m$. These anomalous peaks appeared even after desmearing. In Figure 2, the smeared peaks at $q < q_m$ gradually grew during the heating and cooling cycle, indicating that a proper thermal treatment makes the grain enlarged. Here in this work, we tried to cool the sample with a slow rate in order to develop a large grain.

Figure 3a shows a SAXS pattern of the block copolymer taken with the IP measured at 144.1 °C where the LDS was observed. The first-order scattering peak was perfectly circular because the LDS structure is isotropic.

From this temperature the sample was cooled to 119.6 °C, where the bcc-sphere was observed, at two constant cooling rates: (i) one greater than 100 K/h (the corresponding pattern changing from parts a to b) and (ii) the other of 2.4 K/h (the corresponding pattern changing from parts a to c). Profiles i−iii in Figure 3d are circularly averaged profiles of patterns a−c, respectively. Profile i shows the feature of the LDS structure discussed in the previous section, i.e., broad first-order peaks (marked by a black arrow) and the second-order shoulder (marked by a white arrow). Both profiles ii and iii show the scattering maxima at the positions of q_m, $\sqrt{2}q_m$, and $\sqrt{3}q_m$, indicating the bcc-sphere. However, their 2D scattering patterns were quite different (compare patterns b and c): The first and second-order scattering peaks at q_m and $\sqrt{2}q_m$ appeared as many spots in Figure 2c, while the scattering is roughly isotropic in Figure 2b, indicating that a limited number of large grain composed of the bcc-sphere were developed in the volume irradiated by the incident beam with the slow cooling.

It was observed in Figure 3c that the scattering angle of each first-order diffraction spot was somewhat different. This is not due to the fact that the domain spacing in each grains was different but due to the divergence and the finite cross section of the incident X-ray beam. Figure 4a gives a schematic of our SAXS facility with pinhole collimation. The incident X-ray (drawn by dashed line) diverges toward the 2D detector (imaging plate). Because of this divergence, the scattering that comes from the position a in the sample and that from b have the center of the scattering pattern at different positions on the detector. Consequently, the scattering peaks from the same lattice plane but from different grains in the volume irradiated by the incident beam have effectively different scattering angles as illustrated in Figure 4b. In the hypothetical case of four grains existing with their lattice planes parallel to the incident beam as shown schematically in left side of part b, the diffraction centers will differ about 1.6 mm each other in our SAXS optics (Figure 4a). The lines connecting the diffraction spots at opposite scattering vectors do not intersect at a point. In other words, the diffraction spots having the same center are coming from the same grain. Such a scattering pattern was observed in the right half of Figure 4c (diffraction spots marked with circles). In this case the scattering occurs from the grains of the bcc-sphere whose (001) plane faces normal to the incident beam. The higher-order scattering peaks of $\sqrt{2}q_m$ were observed at a different azimuthal angle of 45° with respect to those of the first-order peaks. All of these observations support the formation of large grains and the bcc-sphere at this temperature.

III-3. Conservation of Grain Structure. Figure 5 gives the SAXS patterns to show a conservation of the grain structures before and after the OOT. After making relative large grains at 119.6 °C where the bcc-sphere is observed (as shown by a limited number of the diffraction spots in part a), we changed the temperature stepwisely to 111.8 °C which is below T_{OOT} (part b) without changing the sample position with respect to the X-ray beam. The pattern in part b was obtained with an exposure time of 60 min after waiting for about 2 h after attaining a constant temperature of 111.8 °C. The same waiting time and exposure time were used to take patterns c and d which were obtained, respectively, by

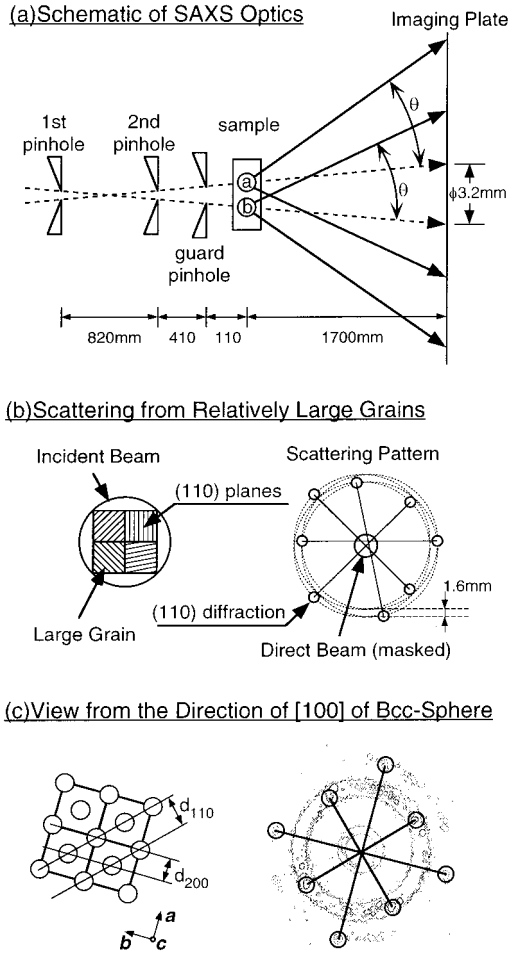

Figure 4. (a) Schematic diagram of the SAXS optics, showing the origin of the shift in the diffraction centers for the diffraction spots of the first-order peaks from the relatively large grains. (b) An example showing four grains having four particular orientations of (110) lattice planes in the volume irradiated by the incident beam and their (110) diffraction spots having different diffraction centers. (c) (110) (200) diffraction spots observed with the incident beam parallel to [001] axis. The diffraction patterns in part c show contour patterns (isointensity lines).

a stepwise increase of temperature from 111.8 to 119.6 °C after taking the pattern in part b and by a stepwise decrease of temperature from 119.6 to 111.8 °C after taking the pattern in part c. The sample position with respect to X-ray beam was kept unchanged for all the patterns in parts a−d. When the temperature was lowered from 119.6 to 111.8 °C, the position of the second-order scattering peaks changed from $\sqrt{2}q_m$ to $\sqrt{3}q_m$, indicating that the microdomain structures changed from the bcc-sphere to the hex-cylinder. The scattering peaks were also observed as many spots, elucidating the large grain structure existed even after the OOT. Furthermore, the temperature was raised again up to 119.6 °C (part c) and lowered back to 111.8 °C (part d). The diffraction spots in the scattering patterns observed at the same temperature were almost identical (compare the patterns between parts a and c and between parts b and d) in terms of their spot size and their position in q-space, indicating that the grain structure was recovered through a **repetitive OOT** process (such as the cylinder−sphere−cylinder OOT process, or the sphere−cylinder−sphere OOT process, etc.) in terms of not only the size but also the orientation of the lattice in each grain.

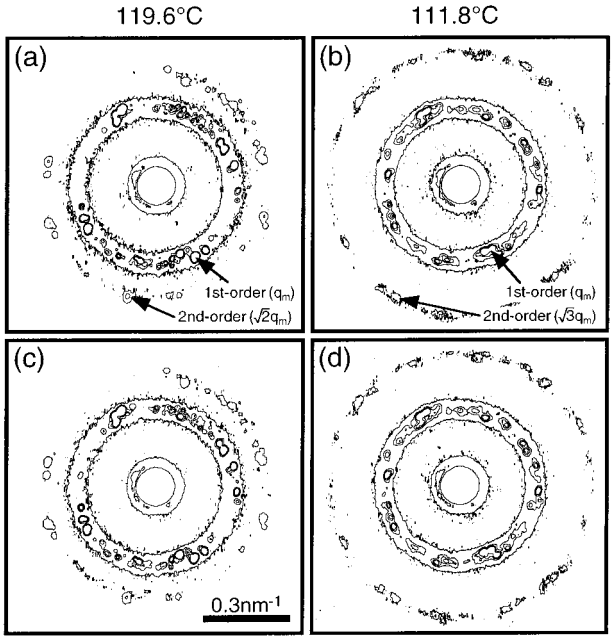

Figure 5. SAXS patterns taken with IP at two typical temperatures, at 119.6 °C (a and c) for the bcc-sphere, and at 111.8 °C (b and d) for the hex-cylinder. The patterns show contour patterns. The measurement was carried out in the order a, b, c, and d by stepwise changing of the temperature, while keeping the irradiated portion of the sample unchanged. The patterns obtained at the same temperature are almost identical, showing the grain structure and orientation of the lattice inside the grains being conserved before/after the transition between the bcc-sphere and the hex-cylinder.

To confirm further the conservation of the grain structure during the OOT, we examined the sample under a polarizing optical microscope (POM) with crossed polarizers. The block copolymer sandwiched between glass slips having a thickness of 0.1 mm was first annealed at 150 °C where the LDS structure exists. With lowering the temperature with a 0.1 K decrement per minute (which corresponds to 6.0 K/h, a minimum cooling step in our apparatus) the sample was cooled to 112.7 °C below T_{OOT} where the hex-cylinders exist. The thermal history employed is schematically given at the bottom right corner of Figure 6 where the arrows labeled with a, b, and c designate the times where the micrographs in parts a, b, and c of Figure 6 were taken, respectively. Figure 6a shows an image due to the form birefringence[28] of cylinders. Above T_{OOT} no clear image was observed as shown in Figure 6b. This is because there is no form birefringence for spherical microdomain structure. When the temperature is lowered back to 112.7 °C (part c), an image almost identical with that shown in part a was obtained. This supports the conservation of the grain structures and lattice orientation during the repetitive OOT, consistent with the observation in the SAXS experiment. These observations indicate that there must be a rule in connecting spheres into cylinders or in disconnecting cylinders into spheres at the OOT. We note here the grains were nonuniform in size, spreading from 10 μm to 0.3 mm in Figure 6.

III-4. Scattering Pattern from a Single Grain. To investigate the rule governing the OOT, we analyzed a scattering pattern from a single grain. To minimize the number of grains exposed by the incident X-ray beam, a sample with a thin thickness (0.3 mm) and an X-ray beam of a small size (0.5 mm in diameter) were used.

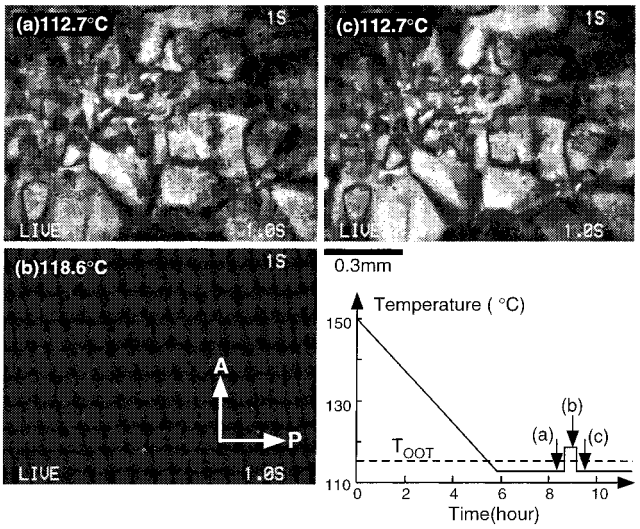

Figure 6. POM images under crossed polarizers taken at 112.7 °C (a and c) where the hex-cylinder is observed, showing an image due to form birefringence of the cylinder. At (b) 118.6 °C where the bcc-sphere is observed, no image was observed. The schematic diagram at the right bottom corner shows the thermal history of the sample. The grain structure was conserved before/after the transition. The dark portions in patterns a and c correspond to those with zero amplitude, while that in pattern b corresponds to that with zero birefringence.

The sample was cooled from ca. 180 to 111.8 °C at a rate of 2.4 K/h and held at 111.8 °C for about an hour. Then by scanning the sample with respect to the incident X-ray beam, we found a 6-fold diffraction pattern at 111.8 °C where the hex-cylinder was observed. The pattern in Figure 7a was taken by exposing the incident X-ray beam for a half hour. Next we changed the temperature to 119.6 °C without changing the sample position with respect to the incident beam, where the bcc-sphere was observed. After waiting for about an hour, the pattern in Figure 7b was taken for a half hour. The hexagonal pattern of the first-order peaks was kept (compare parts a and b of Figure 7).

Figure 7a shows the scattering pattern from almost a single grain of the hex-cylinder. The first-order peaks appeared in a hexagonal pattern (connected by dashed lines) at q_m and the second-order peaks also appeared in a hexagonal pattern at $\sqrt{3}q_m$ at the different azimuthal angles (also connected by dashed lines). The former is the Bragg reflection from the (10) plane of the hexagonal lattice and the latter is that from (11) plane as illustrated in part e. Note that diffraction spots from other grains (e.g., the spot marked with a white arrow in Figure 7a) were also detected. However, here we focus on the single grain showing the hexagonal diffraction pattern. In this situation the incident X-ray beam was parallel to the cylindrical axis as illustrated in part c. The schematic diagram in part e shows the view from the incident X-ray parallel to the cylinders axes which are normal to the plane of paper. The diagram also shows (10) and (11) diffraction planes. In Figure 7a, the lines connected between the spots in opposite scattering vectors intersected at a common center, confirming the scattering of this 6-fold pattern arising from the same single grain. On the other hand, to observe such a 6-hold pattern from bcc lattice, the incident X-ray beam should be parallel to the [111] direction of the bcc lattice as schematically shown in part d. The bcc lattice projected on to the plane normal to the incident beam is shown in part f. The (110) plane shown in part f and two other

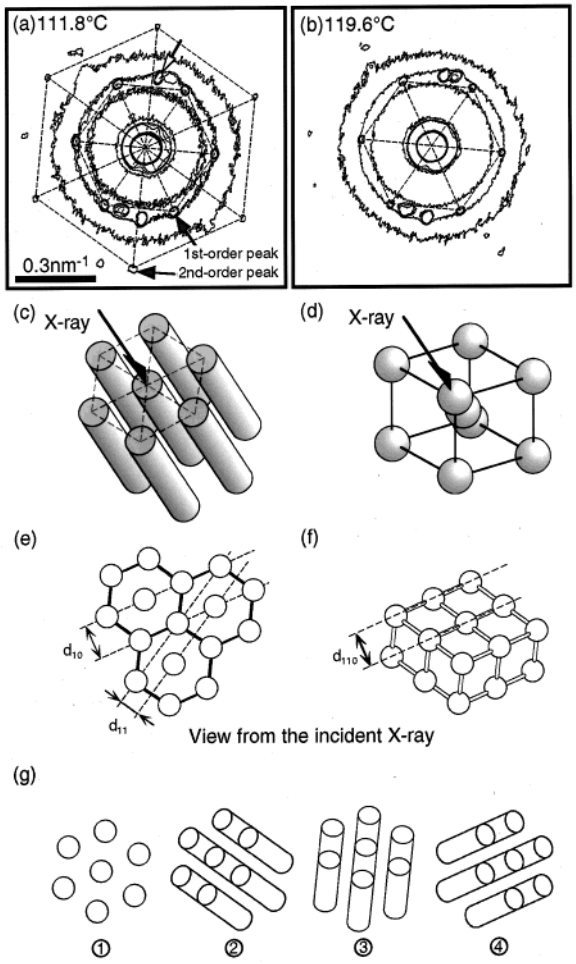

Figure 7. SAXS patterns taken with IP from a single grain at (a) 111.8 °C for the hex-cylinder and at (b) 119.6 °C for the bcc-sphere without changing sample positions, indicating that spheres are formed by disconnecting cylinders with their [111] direction of the bcc lattice parallel to the original cylinder axes. The incident beam is irradiated along the cylinder axis for pattern a (as shown in part c) and along [111] direction of the bcc lattice for pattern b (as shown in part d). The schematic representation of the structure viewed from the direction parallel to the incident beam are shown in part e for the hex-cylinder and part f for the bcc-sphere. Patterns a and b show contour patterns. Part g shows four possible cylinders which are formed by interconnecting spheres lying in the diagonal lines of bcc-sphere with a particular orientation in part f.

equivalent planes give rise to the 6-fold diffraction pattern at q_m as shown in part b. At this point we can conclude that spheres formed by disconnecting a cylinder laid in the [111] direction of the bcc lattice without changing the grain structure.

The bcc-sphere has four identical diagonal lines in the cubic lattice and hence four possible pathways along which the bcc-sphere is transformed into the hex-cylinder. Figure 7g shows these four possible hex-cylinders formed after the transition from bcc-spheres with a particular orientation shown in Figure 7f without changing its orientation during the transition. However, as seen in the conservation of 2D-SAXS patterns in Figure 5 and the conservation of POM micrographs in Figure 6, the lattice orientation in each grains was conserved; e.g., the spheres were connected in such a way that the original cylinder orientation (orientation numbered 1 in Figure 7g) is recovered. We note here if the lattice orientation changed in a part of grain before/after OOT, the scattering patterns would be changed.

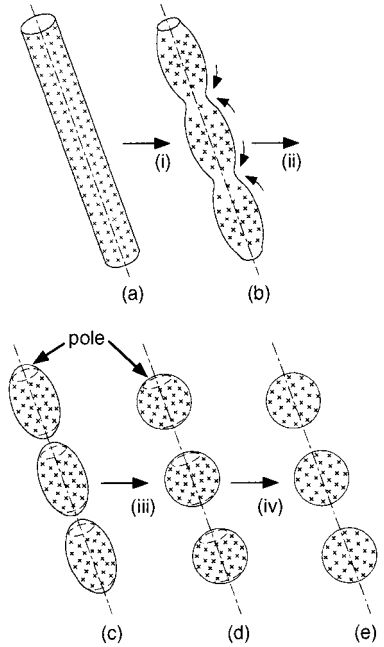

Figure 8. Schematic diagram of the elemental process during the transition from hex-cylinder to bcc-sphere; (i) undulation of the interface (part a to b), (ii) breakup of cylinders into ellipsoids of revolutions (part b to c), (iii) relaxation of domains from the ellipsoids into spheres (part c to d), and (iv) relaxation in junction distribution to attain a uniform distribution (part d to e). The pole where the concentration of the junction points is low may work as a memory of the grain conservation upon the reverse transition from bcc-sphere to hex-cylinder. The small arrows in part b indicate the diffusion of chemical junctions along the interface in process ii.

For example, the cylinders with orientation numbered 2 in Figure 7g and those with orientation numbered 3, which are formed through the sphere-cylinder transition, should have diffraction spots in different positions (in this case a 2-fold pattern with different orientations). In another word, all of the grains should recover original lattice orientation in the repetitive OOT process. Also in the POM micrographs shown in Figure 6, the conservation was observed in terms of not only shape of the grain boundary but also the contrast of the image. The brightness may depend on the angle formed between cylindrical axes and polarizer (or analyzer). If the orientation of the cylinder changed through the repetitive OOT process, the brightness could be different. However we observed the almost same brightness for each grain in the repetitive OOT, which also supports the reverse transition.

IV. Discussion

IV-1. Conservation of Grains and Their Internal Lattice Orientation in the Repetitive OOT. Let us now discuss the origin of the conservation of the grain structure and orientation of the lattice inside the grain in the repetitive OOT. We present below our interpretation. The phase transition from the hex-cylinder to the bcc-sphere is rather straightforward: the cylinder breaks up into spheres with the original cylindrical axis parallel to the [111] direction of the bcc-sphere. This process, which is induced by thermodynamical instability of the cylindrical interface at $T > T_{OOT}$, may have the following elemental processes as shown in Figure 8, where we schematically present a transformation from a single cylinder into a set of spheres and a change in spatial distribution of chemical junctions (presented by x) along

the interface: (i) undulation (as shown from part a to b), (ii) breakup of cylinders into ellipsoids of revolutions (from part b to c), (iii) relaxation of domains from the ellipsoids into spheres (from part c to d), and (iv) relaxation in junction distribution to attain a uniform distribution (from part d to e). These processes involve only local rearrangements of the block copolymer molecules rather than large length-scale rearrangements of block copolymer molecules or microdomains. It may be reasonable for us to assume that process iv is the slowest process.

The reverse transition from the bcc-sphere to the hex-cylinder involves deformation and elongation of the spheres into the ellipsoids and coalescence of the ellipsoids into a cylinder. These processes are driven by thermodynamic instability of spherical interfaces caused by increased segregation power at $T < T_{OOT}$ and lower the interface area and hence interfacial free energy of the domains. However we should note that there are four possible ways in connecting the spheres into the cylinders: as pointed out earlier, there are the four diagonal directions in a cubic lattice. The cylinders numbered 1−4 as shown in Figure 7g could be possible after the transition from bcc-sphere. Why does nature select only one mode (mode 1 in the case of Figure 7g)?

We offer below a possible scenario. Among the various processes involved by the cylinder-to-sphere transformation shown in Figure 8, process iv is the slowest. This may be due to the fact that the translational diffusion of the junctions along the interface is slow,[29,30] because it involves rearrangements of block chains which are interpenetrating each other in the matrix and in the spheres or ellipsoids. Thus, if the time scale t_{obs} of our observation is shorter than the relaxation time t_{jd} in the junction distribution, the spheres or the ellipsoids may have poles aligned along the original cylindrical axes. The poles should have a deficiency in number density of junctions compared with other parts of the domains. The poles should act as a memory for the conservation of lattice orientation within a grain before and after OOT.

Generally when two spheres with "corona chains" (the chains emanating from surfaces of the spheres) come close to each other the corona chains exert entropic repulsion between the spheres. Similarly deformation of the spheres into the ellipsoids as shown in parts a and b of Figure 9 should be also suppressed when it involves entropic repulsion. When the corona chains are distributed on the surface of the spheres the entropic repulsion would be isotropic, and the coalescence of the spheres into cylinders would have no choice of direction. However a series of spheres with poles aligned along the original cylinder axes as shown in Figure 9c should be subjected to the least entropic repulsion upon the transformation into ellipsoids with their major axes parallel to direction connecting the poles (as shown in Figure 9d) because chains between poles have more space due to the deficiency in number of junction points on the pole. These enhance the deformation of the spheres into the ellipsoids and coalescence of the ellipsoids along the line connecting the poles and hence give a deterministic effect on the memory.

IV-2. Comparison with Theoretically Predicted Phase Transitions. Here we compared our experimental results with theoretical predictions. Figure 10 gives the mean-field phase diagram in the weak segregation regime presented by Matsen et al.[19] (thermal fluctuation effects not being included). In the phase labeled with CPS and $Q_{Ia\bar{3}d}$, the close-packed sphere (refers to the spheres packed in a face-centered cubic lattice) and the bicontinuous $Ia\bar{3}d$ cubic (gyroid) are stable, respectively. The vertical dashed line along $f = 0.18$ shows our experimental condition.[31] On this line the theory predicts the hex-cylinder changes to the disordered state via the bcc-sphere and the CPS with decreasing χN, while our experiments indicate the transition from the hex-cylinder to the bcc-sphere, the LDS, and finally to the disordered state, though the disordered state was not attained over the temperature range covered in this study.

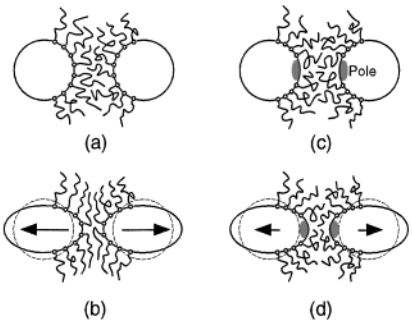

Figure 9. Schematic diagram showing the entropic repulsion of "corona chains" when the spheres with uniform distribution of the corona chains on their interface (a) are deformed into ellipsoids (b) and coalesce into a cylinder and when a series of spheres with poles (having a deficiency in the density of coronar chains) aligned along the original cylinder axes (c) are deformed into ellipsoids (d) and coalesce into a cylinder.

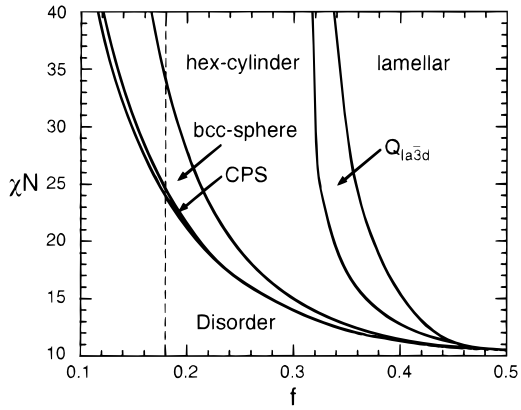

Figure 10. Phase diagram given by Matsen et al. using a full self-consistent field theory. The vertical dashed line shows a trend along which χN may change upon changing temperature under our experimental conditions.

For the purpose of the quantitative comparison, the value of χ_{SI} for the block copolymer is to be determined in the framework of the RPA fitting to the concentration fluctuations in the disordered state. However, the block copolymer used in this study does not show the disordered state within the accessible temperature range (∼180 °C, see Figure 1) free from thermal degradation of the block copolymer. Because of this restriction here, we used the literature value[32]

$$\chi_{SI} = -0.01 + 33/T \qquad (1)$$

with T being the absolute temperature. Note χ depends not only on T but also on molecular parameters such as the composition f and the effective degree of polymerization $r_{n,C}$ (see footnote 28 for the definition). Equation 1 was estimated for our block copolymer ($r_{n,C} = 550$

Table 1. Comparison of the Experimental and Theoretical Critical Values for the Phase Transitions

	experimental		χN for $f = 0.18$	
transition type	T (°C)	$\chi r_{n,C}$	Matsen et al.[19]	Leibler[1]
hex-cylinder/bcc-sphere	115.7	41.2	33.8	29.5
bcc-sphere/LDS	~140 [a]	38.4	NT[c]	NT[c]
LDS/disorder	>180[b]	<34.6	NT[c]	NT[c]
bcc-sphere/disorder	ND[b]		NT[c]	27.2
bcc-sphere/CPS	ND[b]		24.5	NT[c]
CPS/disorder	ND[b]		23.8	NT[c]

[a] Determined as a temperature where the higher-order scattering maxima of bcc-sphere disappeared with an accuracy of ±5 °C. [b] Not detected in this experiment. [c] Not treated in the theory.

and $f = 0.18$) from a master curve of the collection for χ_{SI} measured for many PS−PI diblock copolymer having various f and $r_{n,C}$ values.

The χN value of the transition calculated using eq 1 are summarized in Table 1 together with the theoretically predicted values by Matsen and also by Leibler. The experimental critical value of the transition between the hex-cylinder and the bcc-sphere (41.2) was somewhat larger than theoretical values (33.8 and 29.5). The theories referred here does not include thermal fluctuation effects which remarkably appear around $f = 0.5$; the effects cause the long-range order of the microdomains to be destroyed, and the boundaries between the various ordered phases to shift toward larger χN. However, for our case, $f = 0.18$, the $\chi_{r_{n,c}}$ value is not expected to be affected much by the thermal fluctuation effects.[17] The reason for the discrepancy in the values may be due to an error of the estimation in the interaction parameters presented by eq 1. If so, eq 1 could be modified by simple scaling

$$\chi_{SI} = (-0.01 + 33/T)\frac{33.8}{41.2} \qquad (2)$$

The mean-field disordered phase is expected at $\chi N = 23.8$, which was found to correspond to 250 °C in our block copolymer by using eq 2. This supports our LDS observation to be considered as a fluctuation-induced lattice disordered phase. The fluctuation enlarges the windows for the disordered phase, and therefore the CPS may disappear from the phase diagram. Even if the CPS exists between 23.8 and 24.5, the temperature width is very narrow (about 8 K) to be detected. Moreover the transition between CPS and bcc-sphere requires a change in the symmetry, which may take a long time to occur. All these will make the observation of the CPS phase difficult.

Finally we note here that Matsen et al. also presented the ratio of the wavenumbers for the first-order scattering peaks (q^*). At the boundary between the bcc-sphere and the hex-cylinder along $f = 0.18$ the ratio of q^*_Q/q^*_H is 1.04 with q^*_Q and q^*_H being q^* of the bcc-sphere and the hex-cylinder, respectively. Carefully examining of the scattering pattern in parts a and b of Figure 7 revealed that the q_m for the hex-cylinder was 0.266 nm^{-1} while that for the bcc-sphere was 0.273 nm^{-1}. The ratio, q^*_Q/q^*_H, was 1.026, close to the theoretical prediction. If this simply indicates the isotropic change in the volume, the volume change, ΔV, estimated from the length change (that is the change in $2\pi/q_m$), ΔV, is equal to $1.026^3 \cong 1.08$. This value is enough to cause deformation in the sample and seems to be contradictory to the conservation of the grain structures. One explanation is the existence of the defect in the bcc-sphere to maintain the constant volume before and after OOT. On the other hand Hadjuk et al. claims the displacement of the center of the gravity of the microdomains in the thermoreversible OOT between lamellar and cylinders.[11] In this case, the volume change seems to be no contradiction. To clarify the nature of the transition process, it is also important to investigate the dynamics of the OOT, which will be reported elsewhere.[33]

V. Concluding Remarks

In this paper we presented the thermoreversible OOT between the bcc-sphere and the hex-cylinder of a PS−PI diblock copolymer using SAXS and POM. To investigate the relation between the spatial arrangement of the bcc-sphere and the hex-cylinder, we prepared a sample having relatively large grains which were developed by cooling the sample with a slow rate. The thermoreversibility was confirmed in terms of the morphology. The analysis of the scattering patterns from a single grain revealed that the cylindrical microdomains are burst into spherical microdomains in such a way that the cylindrical axes correspond to [111] directions of the spheres in bcc lattice. In this thermoreversible transition the grain structure and orientation of the lattice in the grain are conserved in the repetitive OOT process. The critical value of χN at the transition was somewhat larger than the theoretically predicted value.

Acknowledgment. We gratefully acknowledge Dr. Tsuyoshi Koga for his useful comments. We thank also to Dr. Jeffrey Bodycomb for useful suggestions on SAXS measurements and to Miss Yuko Kanazawa for synthesis of the block copolymer used in this work.

References and Notes

(1) Leibler, L. *Macromolecules* **1980**, *13*, 1602.
(2) Hashimoto. T.; Shibayama, M.; Fujimura, M.; Kawai, H. In *Block Copolymers, Science and Technology*; Meier, D. J., Ed.; Harwood Academic Publishers: London and New York, 1983; pp 63−108.
(3) Hasegawa, H.; Tanaka, H.; Yamasaki, K.; Hashimoto, T. *Macromolecules* **1987**, *20*, 1651.
(4) (a)Bates, F. S.; Fredrickson, G. H. *Annu. Rev. Phys. Chem.* **1990**, *41*, 525. (b)Hashimoto, T. In *Thermoplastic Elastomers*; Legge, N. R., Holden, G., Schroeder, H. E., Eds.; Hanser, Munich, Germany, 1987.
(5) Sakurai, S.; Kawada, H.; Hashimoto, T.; Fetters, L. J. *Proc. Jpn. Acad.* **1993**, 69 (*Ser. B*), 13; *Macromolecules* **1993**, *26*, 5796.
(6) Sakurai, S.; Hashimoto, T.; Fetters, L. J. *Macromolecules* **1996**, *29*, 740.
(7) Almdal, K.; Koppi, K. A.; Bates, F. S.; Mortensen, K. *Macromolecules* **1992**, *25*, 1743.
(8) Förster, S.; Khandpur, A. K.; Zhao, J.; Bates, F. S.; Hamley, I. W.; Ryan, A. J.; Bras, W. *Macromolecules* **1994**, *27*, 6922.
(9) Khandpur, A. K.; Förster, S.; Bates, F. S.; Hamley, I. W.; Ryan, A. J.; Bras, W.; Almdal, K.; Mortensen, K. *Macromolecules* **1995**, *28*, 8796.
(10) Hajduk, D. A.; Harper, P. E.; Gruner, S. M.; Honeker, C. C.; Kim, G.; Thomas, E. L.; Fetters, L. J. *Macromolecules* **1994**, *27*, 4063.
(11) Hajduk, D. A.; Gruner, S. M.; Rangarajan, P.; Register, R. A.; Fetters, L. J.; Honeker, C.; Albalak, R. J.; Thomas, E. L. *Macromolecules* **1994**, *27*, 490.
(12) Koppi, K.; Tirrell, M.; Bates, F. S.; Almdal, K.; Mortensen, K. *J. Rheol.* **1994**, *38*, 999.
(13) Vigild, M. E.; Almdal, K.; Mortensen, K.; Hamley, I. W.; Fairclough, J. P. A.; Ryan, A. J. *Macromolecules* **1998**, *31*, 5702.
(14) de Gennes, P. G. *J. Phys. (Paris)* **1970**, *31*, 235.
(15) Helfand, E.; Wasserman, Z. R. *Macromolecules* **1976**, *9*, 879.
(16) Ohta, T.; Kawasaki, K. *Macromolecules* **1986**, *19*, 2621.
(17) Fredrickson, G. H.; Helfand, E. *J. Chem. Phys.* **1987**, *87*, 697.

(18) Vavasour, J. D.; Whitmore, M. D. *Macromolecules* **1992**, *25*, 5477.
(19) Matsen, M. W.; Bates, F. S. *Macromolecules* **1996**, *29*, 1091.
(20) Okamoto, S.; Saijo, K.; Hashimoto, T. *Macromolecules*, **1994**, *27*, 5547.
(21) Gupta, V. K.; Krishnamoorti, R.; Chen, Z.-R.; Kornfield, J. A.; Smith, S. D.; Satkowski, M. M.; Grothaus, J. T. *Macromolecules* **1996**, *29*, 875.
(22) Hashimoto, T.; Okamoto, S.; Saijo, K.; Kimishima, K.; Kume, T. *Acta Polym*. **1995**, *46*, 463.
(23) Porod, G. *Kolloid, Z. Z. Polym*. **1951**, *124*, 83; **1952**, *125*, 51; **1952**, *125*, 108.
(24) See, for example: Guinier, A.; Fournet, G. In *Small-Angle Scattering of X-rays*; Mayer, M. G., Ed.; John Wiley and Sons Publishers: New York, 1955; pp 111−120. Actually, the size of the incident beam is finite in our SAXS facility, however, the smearing effect was nearly equal to that for the infinite slit height. About the details, see, for example: Hashimoto, T.; Fujimura, M.; Kawai, H. *Macromolecules* **1980**, *13*, 1660.
(25) Sakamoto, N.; Hashimoto, T.; Han, C. D.; Kim, D.; Vaidya, N. Y. *Macromolecules* **1997**, 30, 1621.
(26) Strictly speaking, relative positions of higher order scattering maximum in a SAXS profile indicate only the lattice type but not the shape of microdomains. To determine the shape, the particle scattering due to the intra-microdomain interference (form factor) should be taken into consideration, though, in our experiment the form factor was not clearly observed. For PS−PI diblock copolymer it is well-known that the spherical domain structure (bcc-sphere or spheres in a face-centered cubic lattice (fcc-sphere)) appears for the A−B block copolymer with $f < 0.17$ (or $f > 0.76$), and the cylindrical structure occurs over the range of $0.17 < f < 0.33$ (or $0.67 < f < 0.76$). (see ref 2−4). In our case of $f = 0.18$, the block copolymer seems to have spherical or cylindrical microdomain structure. These three structures are easy to be distinguished by only the relative positions of higher order scattering maximum (1, $\sqrt{2}$, $\sqrt{3}$, $\sqrt{4}$, $\sqrt{5}$, $\sqrt{6}$, etc for bcc-sphere; 1, $\sqrt{4/3}$, $\sqrt{8/3}$, $\sqrt{11/3}$, $\sqrt{12/3}$, etc for fcc-sphere; 1, $\sqrt{3}$, $\sqrt{4}$, $\sqrt{7}$, $\sqrt{9}$, $\sqrt{12}$, $\sqrt{13}$, etc for hex-cylinder).
(27) Schwab, M.; Stühn, B. *Phys. Rev. Lett*. **1996**, *76*, 924. In this work, however, the state with LDS was defined as the disordered state. We should note, however, that this state is different from the disordered state in lamella- or cylinder-forming block copolymers, simply because the block copolymer in LDS is microphase-separated and the microdomains having a well-defined interface are still static objects, persisting as a structural entity at any time instances in the time scale of our SAXS experiments: they are not dynamical objects which are generated and relaxed with a certain relaxation time. Note also that the microphase-separated state has less entropy than the disordered state free from the microphase-separated structure.
(28) Wiener, O. *Abh. Math.-phys., Kl. Saechs. Ges. Wiss.* **1912**, *32*, 507.
(29) Dalvi, M. C.; Lodge, T. P. *Macromolecules* **1993**, *26*, 859.
(30) Ehlich, D.; Takenaka, M.; Okamoto, S.; Hashimoto, T. *Macromolecules* **1993**, *26*, 189. Ehlich, D.; Takenaka, M.; Hashimoto, T. *Macromolecules* **1993**, *26*, 492.
(31) The composition f is to be considered as a volume fraction of PS, $f = r_{n,\mathrm{PS}}/r_{n,\mathrm{C}} = r_{n,\mathrm{PS}}/(r_{n,\mathrm{PS}} + r_{n,\mathrm{PI}})$. $r_{n,\mathrm{PS}}$, $r_{n,\mathrm{PI}}$, and $r_{n,C}$ are, respectively, the effective degree of polymerization of PS, PI, and whole block copolymer corrected for the asymmetry in segmental volume by $r_{n,i} = (v_i/v_0)N_i$, with v_i and v_0 being the molar volume of the i-block and the reference volume, respectively. Values of 98.8 and 75.6 cm^3/mol were used for v_{PS} and v_{PI}, respectively, and v_0 was calculated by the following equation: $v_0 \equiv (v_{\mathrm{PS}}v_{\mathrm{PI}})^{1/2}$.
(32) Mori, K.; Okawara, A.; Hashimoto, T. *J. Chem. Phys.* **1996**, 104, 7765.
(33) Kimishima, K.; Koga, T.; Hashimoto, T. Manuscript in preparation.

MA991470K